6

Numerical Modelling for Simulation and Planning of Focused Ultrasound Treatments

David Sinden
Fraunhofer Institute for Digital Medicine MEVIS
Max von Laue Strasse 2, Bremen, 28359, Germany

6.1 Introduction

Treatment planning is an optimisation problem which can be approached in one of two ways: as a forward problem or as an inverse problem:

- For a forward problem, given a set of specified initial conditions such as the position of the transducer, phase, amplitude and duty cycle, the fields are simulated. Based on the outcome from these simulations, the operator may decide to proceed with a treatment. This is applicable in cases for which there are no significant organs at risk during the treatment.
- In more complicated cases, treatment planning may take the form of an inverse problem. In this case an intended outcome which delivers the dose at the planned treatment volume while sparing healthy surrounding tissue is defined, and an algorithm will seek to discover the initial set of conditions, such as phase, amplitude duty cycle, exposure duration, which produce a solution very close to the desired outcome. Inverse problems can be solved either directly or indirectly through an iterative process.

For both forward and inverse planning, as stated above, the principle challenge is the simulation of the desired field. In many applications, this requires the computation of acoustic, thermal and (intended) dose models. However, for some, such as those in which the propagation of the acoustic field is nonlinear, solving the inverse problem directly may be not tractable. In this case, treatment planning may require an iterative method, involving the repeated computation of a large number of solutions until convergence close to the desired solution is reached. This places further computational demands on treatment planning.

Thus, the computational cost of performing simulations is important. However, as will be described in this chapter, the implementation of the most appropriate numerical method to model the acoustic, thermal or intended dose field is highly dependent on the application.

DOI: 10.1201/9780429162671-6

Motion compensation[1], segmentation and registration algorithms[2], propagation through bubbly media[3] and the numerical modelling of cavitation or drug delivery[4] are beyond the scope of this chapter, and the reader is referred to the more detailed texts referenced. Instead, this chapter will describe the various models which may be used to model the acoustic, thermal and dose fields, outlining the assumptions employed and how these appropriate the assumptions are in differing clinical contexts.

In the absence of temperature-dependent changes in material properties[5], or boiling bubbles (which lead to enhanced local absorption)[6,7] the acoustic field is independent of any thermal effects. Thus, once the acoustic field has been computed, the thermal field can be computed without a need to update the acoustic field. This reduces the computational demands significantly. However, even allowing for such assumptions, the acoustic field is more computationally demanding than the thermal field, which in turn is more computationally demanding than the 'dose' field, such as that described by the cumulative equivalent minutes formulation (see later)[8]. The thermal simulations are less computationally demanding than the acoustic simulations because the spatial resolution required to compute the thermal field accurately is far lower than that for the acoustic field. The dose field is often simply post-processed from the thermal field. That is, quantities which have been computed from differential equations are simply computed using a simple algorithm which does not require any spatial or temporal information. This chapter will therefore primarily focus on methods for solving acoustic equations which are appropriate for a number of different clinical applications. The governing equations for acoustic, thermal and dose formulations are presented and the limitations discussed, as well as consequent clinical implications. The range of numerical implementations for linear and nonlinear equations are then outlined, and their limitations presented in the context of specific clinical implementations.

6.2 Current State of the Art and Challenges

The pipeline for treatment planning and delivery for external beam therapies can be summarised as follows:

1. Preclinical image acquisition: this may be MRI, CT, and X-ray. Markers that allow the patient to be registered against the images on which treatment planning is performed during treatment ensure that the target can be registered to the planning image in order to deliver the treatment to the intended location.
2. Motion of target is acquired on a different time-scale as the planning images.
3. Image segmentation[9]: in which the preoperative images are partitioned into segments so that organs and objects of interest (*e.g.* tumours) can be identified. At its most basic level, segmentation can be performed by thresholding data and then associating each region with a tissue type based on a table of values.
4. Identification of planned treatment volume, gross tumour margin and Organs at Risk, such as spinal column, significant vascular, nerve or lymphatic structures, healthy tissue etc.
5. Treatment planning: in which output is position and settings of therapy head, such as phase and amplitude of elements, which ensures the intended dose is delivered to the planned treatment volume, while sparing the organs at risk.
6. Registration of target to therapy head to ensure correct positioning for treatment delivery according to the treatment plan.
7. Treatment delivery and monitoring. It is necessary that any intra-operative imaging system clearly delineate the target region, identify any objects within the beam path which may adversely affect delivery (such as bowel gas) and identify the focal region with the target region.

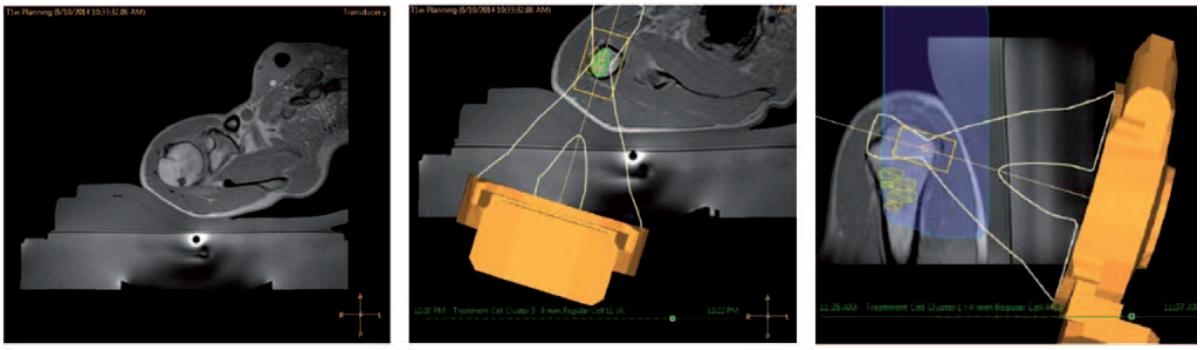

FIGURE 6.1 Targeting of periosteal nerves for pain palliation using MR-guided therapy[10]

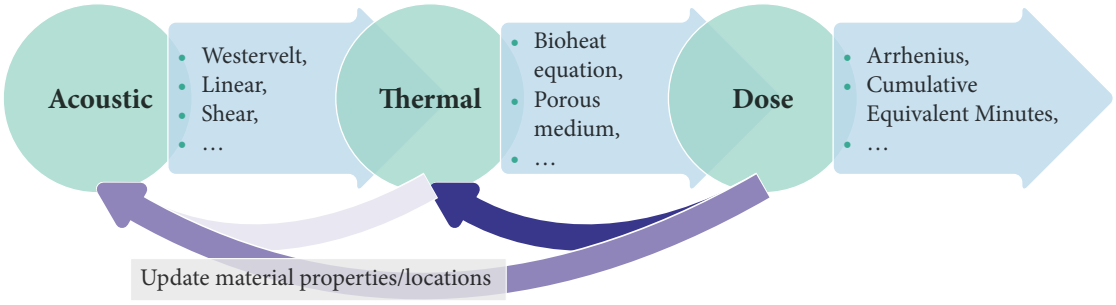

FIGURE 6.2 Schematic of simulation pipeline.

There have been many clinical studies into a range of applications of image-guided therapeutic ultrasound, yet in all reported cases treatment[11–13] planning consists of using the imaging system to locate the focus through a series of targeting shots to ascertain the correct position[14,15]. For ultrasound-guided systems the therapeutic transducer has a central aperture in which a diagnostic probe is confocally placed. The position of the focus can then be overlaid on top of the images. For MR-guidance T_2-weighted fast spin echo images are used to locate the focus. Pulkkinen[16] states that the location of the focus was determined by low power sonications and then the sonications were repeated with increasing power until the desired temperature was reached. After locating an initial focal region and providing a treatment volume, planning software may determine a set of sonication locations to cover the treatment volume. This processed is detailed in Scherrer et al.[17,18], in which the optimisation problem is formulated as two sub-problems: the ideal location of the transducer and the location of the individual focal volumes.

The treatment of the entire volume requires an optimisation routine to ensure complete coverage[19]. If it assumed that the dose delivered is a spheroid or ellipsoid there are many algorithms to ensure complete coverage. Rather than assume that the focal volume will always be ellipsoidal, Fedewa et al.[20] precomputed a number of typical focal volumes, described as a lesion library, at various powers through inhomogeneous tissue for treatment planning in prostate therapy.

Another factor which influences the size of the lesion is the sequencing of the lesions. In order to assure a uniform dose and avoid distortions in the focal volume due to changes in material properties in the beam path, treatment is usually performed from the furthermost plane to the nearest[21].

The selection of the scanning path so that the tumour volume is treated as fast as possible while temperature rise in healthy tissue is minimised would increase the efficiency of ultrasound surgery. Malinen et al.[22] developed a computationally efficient method which optimised sequencing, based on optimal control theory using a quadratic cost criteria to obtain the desired thermal dose in the target region.

The authors showed that treatment times as well as the total applied energy can be decreased from 16% to 43% in comparison to standard sonication sequences.

As mentioned, although treatment planning for therapeutic ultrasound shares many similarities with that for other external beam therapies, the physical mechanisms that come into play in dose delivery, such as thermal and mechanical mechanisms, are different from those due to ionising radiation, and lead to different challenges. The following sections describe some of the challenges, how they affect treatment planning and the techniques which have been proposed to overcome them.

6.2.1 Motion Management

One characteristic feature of therapeutic ultrasound is that the relative size of the focal volume of the dose delivered at clinically relevant conditions is far smaller than the gross tumour volume in comparison to external beam radiotherapy. The precise size and shape of the focal region is determined by a number of factors, such as the transducer geometry and phasing configuration, depth of treatment, tissue properties, power, and frequency. Typically, at low Megahertz frequencies for a clinical transducer, ablated regions may be the size of a grain of rice[23,24]. Thus, an advantage of therapeutic ultrasound is the potential to selectively target pathogenic tissue precisely. However, in cases where the target volume under goes large displacements, such as transcostal applications[25] in which maximum displacements are, as reported by Marquet et al.[26] of the order of 10 mm. Thus, the ratio between the size of the lesion and the amplitude of the motion may be large. Therefore, failure to adequately account for motion in treatment delivery may lead to entire lesions being placed outside of the planned treatment volume.

An additional challenge is to predict the motion of the target for preoperative images. For example, the motion of the liver can be predicted due to periodic forcing from the diaphragm. However, the exact motion of the diaphragm, the coupling between the diaphragm and the liver, and the constraints due to the ribs and skin are difficult to know precisely.

For simple cases, motion management can be performed based on the assumption of incompressibility, in which case organs simply undergo translation in coronal, sagittal and transverse planes, or more complicated deformable models applied[27,28]. In such cases complex finite element simulations are employed to predict organ motion. Naturally, such methods do not capture the full complexity of the situation. For example in transcostal applications the intercostal spacing changes in time as the ribs move, or sliding motion of the lungs against the rib cage[29,30]. Another approach is to compute the deformation due to external (such as motion or acoustic radiation force) and internal (such as tissue compression or expansion due to heating) effects and apply this on to the computational domain, then interpolate the updated field onto the computational grid[31].

An associated problem is that it may be time consuming to treat large volumes. Lorton et al. derived an approach to exploit the motion of the target to increase the volume of a lesion, to reduce treatment times[32]. Note that In this case, drift of organ position may lead to targeting errors[33]. Furthermore, for treatments at low intensities for long durations, the expression of heat shock proteins[34] may inhibit treatment.

6.2.2 Material Properties

Another significant source of uncertainty in treatment planning which can lead to errors in treatment delivery is what values for the material properties (density, speed of sound, nonlinearity, attenuation parameters, thermal conductivity and specific heat parameter *etc.*.) are used within the governing equations.

From pre-operative planning images, typically either CT or MR, tissue types must be identified. For CT images, in the simplest case, this may be performed by thresholding the images, then mapping from

Hounsfield units to density, which are then semi-automatically assigned a tissue type with corresponding acoustic and thermal properties, from the literature, *e.g.* Duck[35]. For MRI, depending on the sequencing, a similar procedure assigns acoustic and thermal properties based on a look-up table which matches T_1, T_2 relaxation times and spin density to tissue type. Aside from thresholding, there are a plethora of more advanced techniques which perform the segmentation — such as using machine learning, using partial differential equations, edge detection, Markov-chains *etc.*[9].

A significant challenge is that, in contrast to radiotherapy, ultrasound can significantly interacts with the propagation medium: through absorption and nonlinearity the medium alters the beam, and the beam alters the medium. As mentioned, for computational reasons, this is often neglected, and the material properties do not change throughout the duration of the exposure. However, the changes in acoustic properties with temperature is used to monitor treatment delivery. The review article by Lewis et al.[36] outlines the main mechanisms for thermometry and dose monitoring and their respective advantages and disadvantages.

Thus, detailed knowledge of the thermal and acoustic properties of soft tissue are required, as well as how they change with temperature. Methods to determine the required patient-specific parameters *pre-operatively* are, at present, lacking.

Neufeld[37], Vaughan and Hynynen[38] and Suomi and Cleveland[39] all investigated the effect of uncertainty of material properties on simulation. In the context of transcranial ultrasound, Vaughan and Hynynen investigated variations in speed of sound and CT data errors, such as skull thickness, and found that the predicted pressure can vary by a few percent at the focus. Neufeld investigated variations in attenuation, speed of sound and density for linear propagation through water and found that variations to the speed of sound effected the magnitude and also shape of the focal volume. Recently, using patient data, Suomi and Cleveland[39] found that attenuation, from the perinephric fat around the kidneys[24], and focal splitting due to refraction lead to significant reduction in heat deposition rates. The authors showed the effect of reflections from soft tissue interfaces was negligible.

While changes in material properties can lead to distortion of the beam, through the thermal lensing effect[5,40], the most pronounced instance of the tissue affecting the beam shape is when cavitation occurs. The presence of bubbles at a desired location can locally enhance heating rates, potentially reducing sonication times. However, controlling the location is problematic — as large pre-focal echogenic bubbles can distort the focal beam shape.

In some applications, such as transcostal therapies, the presence of bone can be avoided through ray-tracing or more advanced methods[25]. However, for transcranial applications, propagation through bone is unavoidable. In such cases, aberration corrections[41] are employed to ensure that the acoustic field has a coherent focus at the intended location.

The presence of bone presents two challenges: firstly, as wave propagation in hard tissue supports shear waves, which are readily absorbed. Thus, within treatment planning models, equations which model elastic waves must be coupled to the acoustic wave equations. Secondly, thermometry, especially MR-thermometry, is a challenge in both fat and bone, so that the validation and verification of thermal fields remains a challenge[42].

A potential challenge for treatment planning in applications in which there is a significant impedance mismatch, such as an air/water interface or soft tissue/bone interface, is the formation of standing waves due to multiple reflections. Standing waves are formed due to the constructive interference of waves of similar amplitude propagation in opposite directions. Standing waves formation may lead to localised heating due to constructive interference, or distort the focus as the reflected sound waves affect the vibrations of the transducer. The formation of standing waves presents challenge in transcranial applications in which standing waves can form[16] (i) between the transducer and the skull (ii) within the calvaria and (iii) within the brain. Techniques such as frequency sweeping[43], or random phase modulation[44] have been employed to suppress standing wave formation.

6.2.3 Vasculature

Thermal therapies may be compromised by the presence of large blood vessels, which advect heat away from the target site[45]. In a review of the safety and efficacy of ablative treatments on the hepatic and biliary system, Mann et al.[46]. state that vessels larger than 3 mm in diameter acted as a heat sink. Hynynen et al.[47]. state that presence of large vessels complicates treatment as occlusion of vessels will have an effect on healthy tissue. As mentioned, the acoustic field is independent of temporal effects. Thus, the effects of the acoustic field on the flow, known as acoustic streaming, are neglected. Kamakura[48] investigated the effect of acoustic streaming in an axisymmetric case in which a vessel ran along the axis of propagation, and found slight enhancements in means flow due to the acoustic field, but a strong dependence on nonlinearity. Solovchuk[49] investigated clinically relevant vessel configurations, using a linear Westervelt equation[50] and bioheat equations[51], for acoustic and thermal fields coupled to a non-linear Navier–Stokes equations for the flow, which was solved using a finite-element method. The authors found that for large blood vessel both the convective cooling and acoustic streaming can significantly change the temperature field and consequent thermal lesioning close to the vessel walls. However, the effect was highly localised.

6.3 Acoustic Equations

Differing applications may require different governing equations, based on the assumptions which can be made. The central question therefore is, given the treatment, what is the appropriate governing equation and solution method?

One common feature is that the initial propagation from the transducer will be through water at a single frequency, and that in the near-field, the propagation will be linear. Near the focus the intensities may be sufficiently great so that the effects of nonlinear wave propagation cannot be neglected.

The governing equations for the simulation of ultrasound wave propagation can be modelled using the Navier–Stokes equations and an appropriate constitutive equation — *i.e.* an equation which relates a pair of the variables, such as the dependence on the density to the speed of sound[50,52]. This would be extremely computationally expensive, but would not introduce any approximations into the simulations, and would yield conservation laws which would aid verification of numerical implementations.

The Westervelt and KZK equations can be derived from the Navier–Stokes equations as follows: the first approximation is to assume potential flow, $\mathbf{v} = \nabla\Phi$, where Φ is the potential function. This approximation assumes that vortices and shear waves are negligible. The second step is to consider small perturbations of the variables, and assume the acoustic Mach number is small, so that higher-order terms can be neglected. The acoustic Mach number is defined as the ratio of the characteristic particle velocity to the speed of sound in the fluid, *i.e.* $\varepsilon = u/c$. This step yields so-called *weakly nonlinear equations*[53]. If the medium is homogeneous the Kuznetsov equation[54] is derived. Then, discarding thermal effects yields the second-order wave equation[55]. Assuming there are no local effects, then the Westervelt equation is derived[56].

If the acoustic field propagates primarily in a single direction, it is reasonable to make the parabolic approximation. This assumption is valid when there are no scatterers in the path of the beam. The parabolic approximation asserts that in the appropriately retarded reference frame, *i.e.* $\tau = t - z/c$, the wave profile varies slowly in all directions and extremely slowly in the direction of motion. This is enforced by introducing a generic small parameter ν, of similar magnitude to the (acoustic) Mach number ε, and writing Φ as

$$\Phi = \Phi\left(\tau = t - \frac{z}{c},\ x = x\sqrt{\nu},\ y = y\sqrt{\nu},\ z = \nu z\right) \quad \text{where } \nu \ll 1, \tag{6.1}$$

and neglecting terms of the order of ν^2 and higher. In the above formulations, the transformation assumes that propagation is in the z direction. Note the change of coordinates is exact; the approximation is by discarding $\mathcal{O}\left(\nu^2\right)$ and higher terms.

Due to its relative simplicity and limitations on the computational tractability, the KZK equation, and increasingly the Westervelt equation, are the most commonly used models for simulation of therapeutic ultrasound fields. This is because the KZK and Westervelt equations are the simplest acoustic models which capture the three key phenomena of diffraction, nonlinearity and attenuation.

- Diffraction is the spreading of the wave as it propagates from a medium.
- Nonlinearity is the change in the wave form as it propagates through a medium. This is because the speed of sound varies with the magnitude of the pressure. That is, in compression the wave speed is greater than in refraction. This can lead to wave-steepening and shock-like waves.
- Total attenuation is the loss of acoustic energy as the wave propagates through tissue due to absorption and scatter. Attenuation in tissue is known to be dominated by absorption. In the low megahertz frequency range, the scatter component of attenuation in soft tissue accounts for about 10% to 15% of the total attenuation. The two main mechanisms for absorption, which are dependent on the material, are:
  - Thermoviscous heating: this is the primary mechanism for absorption in water. It is due to a combination of internal friction in a fluid and the heat conduction. The absorption in this case follows a quadratic dependence on frequency.
  - Relaxation processes are the dominant mechanism for absorption of ultrasound in tissue. Relaxation refers to the time required for a medium to establish equilibrium in a new thermodynamic state produced by a change in one or more of the internal degrees of freedom, *i.e.* rotational, vibrational or chemical modes. During each compression cycle, there will be a net transfer of energy from the sound wave to the internal degrees of freedom, attenuating the amplitude of the wave.

While both types of absorption are frequency dependent, there is a significant difference: viscous heating follows a quadratic dependency on frequency, whereas the absorption of ultrasound through relaxation processes follows a power-law dependency. The latter is computationally far costlier to accurately model and influences not only the solution method employed, but also the governing equation[57].

Accurate computation of the absorption is important in therapeutic applications as the preferential absorption of higher harmonic components means that nonlinearity leads to a more concentrated energy deposition in a smaller region, thus higher focal temperatures. Other consequences are a narrower focus and smaller sidelobes, as well as a restricted ability to electronically steer a phased array.

The therapeutic application determines the choice of governing equation and the numerical solution employed to solve it. However, the numerical solution essentially determines how the power-law absorption is implemented.

A finite sum of relaxation processes can be easily implemented in finite-difference time-domain simulations[57,58], whereas for pseudo-spectral methods (either forward-marching in space, or k-space methods which step forward in time) can be handled by assuming a continuous distribution so that the absorption follows a power-law dependence on frequency[59]. This power-law dependence can yield an operator which may be either a fractional Laplacian in the spatial variables[60], or a fractional operator in the time-domain. If a continuous distribution of relaxation processes are assumed in time-domain simulations, an integral or convolution operator[61] can be employed to handle the power-law absorption.

A key difference between the KZK and the Westervelt equations is that the KZK equation is rotationally symmetric — that is the Westervelt equation computes the field in three dimensions whereas

the KZK equations computes the field in two spatial dimensions. An advantage is that rapid calculations can be made for calibration in symmetric transducers exposing through homogeneous layered materials. However, the simplicity of the KZK comes at the cost as the assumption of rotational symmetry severely limits the clinical applicability of the KZK equation, for example, the KZK equation cannot adequately model steered beams from phased arrays.

The paraxial approximation limits the applicability of the model: in theory the KZK equation is valid only for wave travelling at 16 degrees off the axis of propagation from a focused transducer, *i.e.* f-numbers above 1·5. Thus, it is less accurate in the near-field and off-axis. However, while in practice the KZK equation has been found[62] to be in good agreement for f-numbers as low as 1.0. Soneson[63] performed a sensitivity analysis and found that up to 22 degrees the error is 5%.

If the medium in which the sound is propagating is weakly inhomogeneous, then reflections are a minor effect[39] and the KZK equation is sufficient. In many applications, especially in the upper abdomen, intervening bone can cause strong reflection and lead to tissue damage far from the focus. For patient safety, the strength of the reflected beam must be estimated. This does not exclude the use of the KZK — a second field can be introduced to describe the reflected beam — but the formulation becomes more computationally demanding[64].

While the use of either the Westervelt or KZK equations is widespread, the implementation of the numerical method which is used to predict the acoustic, thermal or intended dose field is highly dependent on the application.

For example, for low intensity exposures, nonlinearity can be discarded, whereas for high-intensity exposures, nonlinearity must be included in treatment planning routines, as mentioned the higher harmonic components will be preferentially absorbed. As will be described, the inclusion of nonlinearity presents a significant computational challenge.

Another example is the exposure duration; for long exposure durations it can be assumed that the exposure is for a continuous wave, whereas for short exposures, this cannot be assumed. The assumption of continuous wave exposures allows for a range of number techniques which can accelerate the computation, and provide simplifications in the computation of the absorption.

Two aspects which are, at present seldom to acoustic computational models are nucleation of inertial cavitation and phase changes, such as boiling or emulsion. The presence of large vaporous echo-genic bubbles, which are associated with boiling, have be used as a monitoring device using B-mode imaging[36]. However, for high void fractions, *i.e.* over 5%, the effect of the presence of a cloud of bubbles on wave propagation, local absorption and heating is numerically challenging[65,66]. This is because bubble oscillations and interactions occur on smaller time scales then the frequency of the wave propagation, increasing computational requirements. Furthermore, the inclusion of bubble oscillations naturally leads to time-domain computations and the bi-directional coupling of the thermal and acoustic fields.

6.3.1 Shear Waves

In solid tissue such as bone, the wave propagation is no longer purely longitudinal, but may support shear waves[67]. Shear waves can be generated at an oblique interface between solid and fluids. Shear waves are rapidly absorbed and as such do not propagate far in soft tissue. Thus they provide a highly localised heat source. Shear wave heating can use for palliative treatments of bone metastases by damaging periosteal nerves. A pair of parameters, such as Lamé parameters or bulk modulus and shear modulus can be used to characterise the propagation in solid material.

Poroelastic models, with slow and fast waves may provide more detailed and accurate models of wave propagation through bone that solid materials. McGarry et al.[68] describe the differences between the two models in the context of MR-elastography. A challenge is that the poroelastic properties of bone are dependent on bone density which may be patient specific. Poroelastic modelling requires additional

parameters[69] — porosity, hydraulic conductivity and apparent density.

6.3.2 Full Wave Evolution

Full-wave evolution refers to the ability to compute propagation in all directions. Not all simulations are full-wave because of either the formulation of the governing equations or the numerical implementations to solve them.

Computations can be significantly accelerated by representing the some portion of the waves by an orthogonal basis, such as a Fourier series or Chebyshev polynomials. Such methods are referred to as pseudo-spectral. There are two main types of pseudo-spectral methods:

- Pseudo-spectral time-domain methods, also known as k-space methods. These methods formulate the governing equation in terms of a time-derivative and represent all of the spatial components of the wave via a Fourier series. For example, the pressure would be written as $p\left(x, y, z, t\right) = \hat{p}\left(k_x, k_y,\ k_z,\ t\right)$, where $\hat{p} = \mathcal{F}\left(p\right)$ is the spatial Fourier transform of the pressure and the governing equation would take the form $\frac{\partial \hat{p}}{\partial t} = f\left(\hat{p}, k\right)$. The time derivative can then be approximated by finite-differences so that the next time-step can be computed from the previous time steps.

- Pseudo-spectral spatial marching schemes: those which compute the entire time history in a plane orthogonal to the direction of propagation and march forwards in space

Hence spatial marching schemes rely on defining the field (pressure and/or velocity) for all times on a particular plane in space. This initial planar field is stepped forward in space to find the solution on a series of planes. The initial source plane is usually determined by holography[70]. A full-wave approach has the field defined everywhere in space at the initial time, and the field is then evolved forward in time, with appropriate time-varying boundary conditions at the transducer surface

Propagating in time may be more intuitive and can handle reflections and scatter without too much overhead, whereas propagating in space provides the advantage of being able to handle dispersion and propagation across interfaces efficiently[71,72]. The primary advantage of spatial marching schemes is that they are efficient for continuous wave exposures as they compute the entire time history of the wave. However, marching forward in space is only applicable in cases for which reflections are not important, and when exposure durations are sufficiently long to assume continuous wave exposure. In the case of continuous wave exposures, forward-marching schemes assume that the material properties do not change in time. For strongly heterogeneous media, Gu and Jing[72] derive phase and amplitude corrections which are exact in the one-dimensional case, as well as computed multiple reflections.

The primary advantage of pseudo-spectral time-domain methods is that they can stably and accurately compute spatial derivatives with a small number of points per wavelength. However, the presence of discontinuities, such as between soft tissue and bone requires additional computational techniques, such as Fourier continuation[73] or Gegenbauer reconstruction[74], to handle discontinuities. Yet for soft tissues, in which local medium properties show small variations, the method is sufficient to compute acoustic fields accurately and efficiently. A computational cost is that the visualisation of the evolution of the acoustic field requires storing the entire state of the acoustic field at each time point.

Pseudo spectral methods requires periodic boundary conditions which are inappropriate for therapeutic ultrasound. However, this can be overcome by incorporating Berenger's perfectly matched layer formulation. In contrast to many boundary conditions which impose conditions on points on the boundary, the perfectly matched layer formulation imposes a condition on an artificial domain. The material properties within the domain are chosen so that they fully damp waves which enter into the domain without causing reflections back into the computational domain[75,76]. The specific implementation of the

perfectly matched is dependent on the coordinate frame used. Although more computationally expensive than absorbing or reflecting boundary conditions[77], the perfectly match layer is perhaps the mostly widely used boundary condition as it allows the implementation of pseudo-spectral methods, and provides physical realistic results without numerical artefacts.

6.4 Thermal Equations

The thermal field is computed using the Pennes Bioheat Transfer Equation[51]

$$c_v \rho \frac{\partial T}{\partial t} = \nabla \cdot (k \nabla T) + q_a + q_s + q_c + q_m + \omega_p \left(T - T_\infty\right), \tag{6.2}$$

where c_v is the specific heat capacity, ρ is the density, k is the thermal conductivity, source terms q are heat sources due to absorption, shock-enhanced heating, cavitation and metabolic heating respectively, ω_p is the bulk perfusion parameter and T_∞ is the ambient temperature. The effect of perfusion appears as an isotropic, homogeneous cooling term which reaches instantaneous thermal equilibrium.

One deficiency of this model, noted by Pennes, is its assumptions are only true for heat transfer between blood and tissue in the capillaries. This was found to be inaccurate by Chen and Holmes[78] who showed that, in a simplified model, equilibration between blood and tissue occurs primarily in vessels of 0.2 – 0.5 mm diameter, and not in the capillaries (which have a diameter in the micron range). Nonetheless, the Pennes' model is straight forward to implement, and produces reasonably good agreement with experimental data in regions without large blood vessels. The primary advantage of Pennes bioheat equation is that the inclusion of a bulk perfusion term simplifies the model significantly, allowing for comparatively rapid simulations to be performed.

All these models are single field. An alternative approach is to consider the evolution of three temperatures fields — tissue, venous and arterial. This approach was explored by Keller and Seiler[79] and several modifications have since been proposed. These are expected to be more accurate, but rely on deriving effective medium properties of the blood flow for thermally significant vessels which may not be visible. However, asymptotic homogenisation techniques can rigorously model vascular structures on a scale which is smaller than the resolution provided by medical imaging[80].

Discrete modelling is possible for thermally significant blood vessels which can be imaged[81]. This is important since vessels greater than 1 mm in diameter can significantly affect the thermal dose delivered during ablative therapies, due to advected heat transfer. This can lead to unwanted tissue-sparing (increasing the risk of disease recurrence), asymmetric dose and the over-treatment of healthy tissue. Furthermore, regions with large, thermally significant vessels require a greater ultrasound exposure, involving either higher intensity, or longer treatment times. A reduced model, which includes the effects of discrete vasculature without computing the effects of advected blood flow is to simply assume through a combination of low thermal conductivity and high flow rates, the blood does not heat up and so model vessels as having a fixed temperature. Thus, in this case, like the Pennes' model, the vessels act as heat sinks, but the effect is not isotropic[82].

6.5 Dose Formulations

The primary measure of dose in therapeutic ultrasound is the cumulative equivalent minutes formulation. It is based on a first-order irreversible Arrhenius-type rate equation[83] for protein denaturation. It

is assumed that a small element of is comprised of tissue which is either alive or dead, and the rate at which tissue is denatured is proportional to the temperature. This yields an integral for a dimensionless, time-dependent irreversible damage function, $\Omega(t)$,

$$\Omega(t) = \int_0^t A e^{\frac{E_a}{RT(\tau)}} \, \mathrm{d}\tau \tag{6.3}$$

where R is the universal gas constant, E_a is the activation energy and A is a constant of proportionality which corresponds to the collision frequency. In this case damage refers to denaturation of proteins within cells[84].

There are extensions to the standard Arrenhius model, for example by O'Neil et al[85] or Xu and Qian[86], which include multiple states in which tissue may be alive, (reversibly) damaged or (irreversibly) denatured. These more advanced models are often used in thermal-deformation models which relate damage to tissue expansion and contraction to tissue denaturation[87].

A related concept is the cumulative equivalent minutes formulation , which is based on empirical evidence which suggests that there is a relationship between sets of exposure durations and temperatures of the form

$$t_1 = t_2 R_0^{(T_1 - T_2)}. \tag{6.4}$$

The relations states that for a given exposure temperature, T_2, and duration, t_2, the equivalent exposure time, t_1, at the new exposure temperature, T_1, is given by the exponential relationship stated above. The exponent, empirically derived from the biphasic Arrenhius plot is given by

$$R_0 = \begin{cases} 0 & \text{for} \quad T < 39^\circ \\ 0.25 & \text{for} \quad 39^\circ \leq T < 43^\circ \\ 0.5 & \text{for} \quad T \geq 43^\circ \end{cases} \tag{6.5}$$

For time-varying temperatures, the equivalent time is obtained by summing contributions from different temperature-time combinations:

$$\mathrm{CEM}_{T_{\mathrm{ref}}} = \int_0^{t_\infty} R_0^{T_{\mathrm{ref}} - T(t)} \mathrm{d}t. \tag{6.6}$$

The most widely used formulation for thermal ablation is a CEM_{43} of 240, which corresponds to raising the temperature to 43°C for 240 minutes. The relationship between the Arrenhuis and CEM formulations is explored by Pierce[88].

Thus, from the computed thermal field the dose field computation of the CEM_{43} integral for a small unit of tissue is either above the threshold or below. If it is above the threshold the value of the dose field at this small unit of tissue does not need to be computed at the next step, if it below the dose must be updated at the next time step.

For small induced temperature rises, an equivalent minutes formulation which corresponds to the delivery of dose for hyperthermia, rather than ablation, is to heat tissue at 43°C for 90 minutes[89].

For exposures associated with extreme intensities[62] (*i.e.* above 20,000 W/cm^2), and short exposure times, the time to achieve a CEM_{43} of 240 may be of order of microseconds. The mechanism for cellular damage in such short exposure times is likely to be mechanical damage from boiling[23,90]. Such short exposure times may negate the effects of two significant sources of uncertainty in treatment delivery in perfusion and tissue motion as they occur over longer time scales. However, these high intensities may lead to difficulties in predicting lesion formation due to the random nature of cavitation distorting the shape of the focus.

6.6 Linear models for ultrasound wave propagation in tissue

6.6.1 Ray Tracing

Perhaps the simplest approach to simulation is to neglect diffraction and nonlinearity and consider ray-tracing, *i.e.* geometrical acoustics. Ray-tracing is accurate in the high-frequency limit, which is when the width of the sound beam is much larger than the wavelength. Ray-tracing algorithms are fast, easy to parallelise and can handle inhomogeneous and discontinuous media. Such methods provide a useful measure of transmission losses due to reflection, as well as the influence of shift of the focus due to refraction due to differences in sound speed between differing media, such as water/skin interface[91]. However, the precise field in the focal region is difficult to determine. As such they may provide a useful first approximation to iterative nonlinear solvers. Furthermore, ray-tracing is a useful approach when considering focusing of phased-arrays beyond targets, such as the ribs, in which certain elements of a phased array are directly incident on the ribs. Alaniz et al.[92] used ray tracing to calculate thermal lensing in HIFU, *i.e.* defocusing of the focal region due to heating.

6.6.2 Rayleigh–Sommerfeld Method

The Rayleigh–Sommerfeld method is a time domain method which, although derived under a number of restrictive assumptions regarding the domain, allows for the modelling of a number of transducer geometries. The model is formed under two assumptions: firstly, that the acoustic field is generated by piezoelectric elements which are planar and within an infinite baffle and secondly that the waves propagate linearly through an infinite, homogeneous domain. Using these assumptions, a Green's function formulation is employed.

Typically quadrature methods are employed to characterise the source, so that, each element of the phased array is discretised into a finite number of small point sources. The computation of the acoustic field at a given point is then comprised of the sum of the contributions from each point source.

To over-come some of the limitations of the Rayleigh–Sommerfeld method a number of modifications have been implemented. For example, it is not possible to compute the acoustic field at the source points as the Green's function is singular, consequently the computation of the near-field is problematic — especially at higher frequencies. To over-come this limitation, fast nearfield methods have been developed for simple transducer geometries. This method replaces the double integral in the Rayleigh–Sommerfeld method with a rapidly converging single integral[93].

Although the applicability of the model is limited by the restrictions imposed by the use of the Green's function, the Rayleigh–Sommerfeld method is simple to implement, parallelisable and can handle complex transducer geometries and temporal variations in field strength. The Rayleigh-Sommerfeld method is therefore widely used and can give reasonable agreement with measurements at low pressures.

6.6.3 Angular-Spectrum Methods

The angular spectrum method is a frequency-domain method which, from a source-plane, usually perpendicular to the direction of propagation, containing the phase and amplitude of the field, propagates the plane forward (or backwards) in space in the direction of propagation[94]. The source information can be acquired experimentally, or computed numerically, *i.e.* using the Rayleigh–Sommerfeld method. The angular spectrum method naturally handles dispersion and attenuation, and is commonly employed to model the diffraction operator in nonlinear simulations which used operator splitting[95]. The method is relatively straight-forward to implement and is computationally efficient, so that large domains can be

modelled. However, it implicitly assumes a direction of propagation which may not be the case for hemispherical devices used in transcranial applications. It has been extended to inhomogeneous media[96] for materials which are weakly inhomogeneous, i.e. through computational domains which do not contain any significant discontinuities in acoustic impedance.

6.6.4 Finite-Difference Time-Domain Methods

Finite-difference time-domain methods are relatively straight forward to implement and have even been used to simulate large scale models using graphic processing units[97] (GPUs). In order to approximate spatial derivatives, simple first-order accurate differencing schemes typically only require a few terms to be stored in memory. However, finite-difference methods require high spatial resolution, typically 10 points per wave length[98]. This becomes computationally expensive when nonlinear wave propagation needs to be included. Due to the preferential absorption of high-frequency components of a nonlinear wave, it is likely that a linear simulation, or not computing all harmonic components, may underestimate the thermal field. Soneson and Myers[99] calculated thresholds at which nonlinearity became significant using the KZK equation.

6.6.5 Boundary Integral Equations

Boundary element methods exploit the fact that the linear wave equation has a Green's function which, in some cases, can be used to derive a solution over a given surface rather than a volume. That is, from a given incident field, the total acoustic field from the incident and scattered fields can be easily post-processed from the field which has been computed on the surface of the scatterer. This is naturally performed in the frequency domain, so that the governing equation is actually the Helmholtz rather than the linear wave equation. This has been performed, and incorporated into a constrained optimisation scheme to perform treatment planning in the case of transcostal surgery for a phased array[25]. In this case the phase and magnitude of each element of a phased array was determined so that spatial-peak intensity was maximised at the intended focus, while the energy deposited on the ribs was minimised using a nonlinear least-squares method. The formulation assumes a homogeneous media, but it is possible to couple boundary element and finite element models, to account for tissue inhomogeneity and thermal fields. However, by solving the Helmholtz equation, it is assumed that there is continuous wave exposure, so that pulsed or short tone-bursts cannot be modelled.

Although the boundary element method solves a linear system of equations, Groth et al[100] coupled a system of harmonic equations within a series of nested domains to solve for a nonlinear acoustic field. A cascade of Helmholtz equations can be solved successively at each harmonic of the fundamental frequency with source terms which are products of lower harmonics.

6.6.6 Machine Learning Methods

An approach is to develop a neural network which is trained to approximate the solution of the acoustic field given by a propagation equation[101]. Within the context of therapeutic ultrasound, such physics-informed neural networks have been used to model the linear, continuous-wave two-dimensional acoustic fields which propagate through a skull model[102], but are not necessarily limited to linear propagation. An advantage of such an approach is that the model can be trained to approximate the acoustic field based on a large set of training data, and then applied to patient data to rapidly predict the acoustic field without computing the full acoustic field.

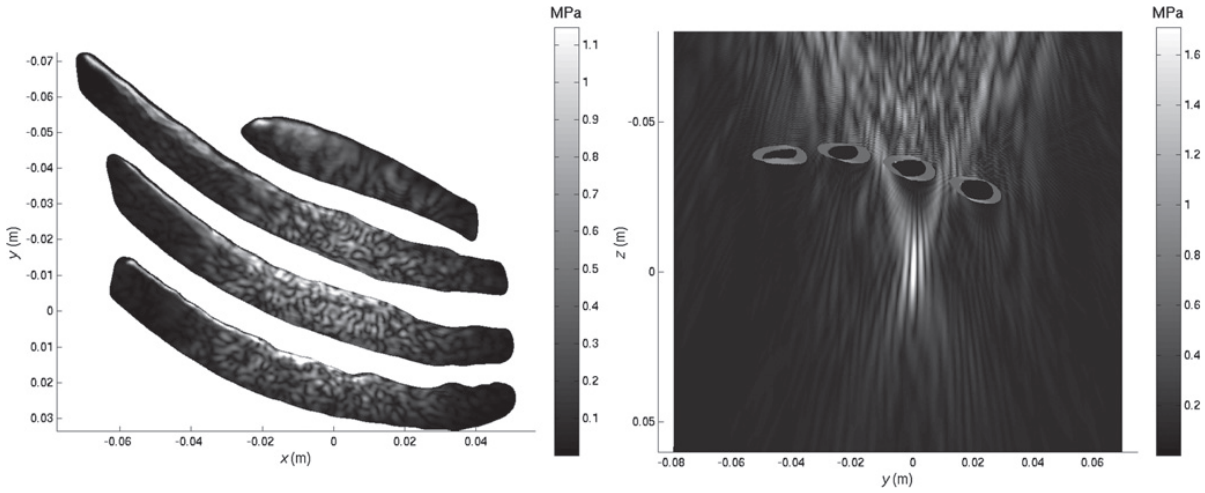

FIGURE 6.3 Acoustic pressure magnitude incident on ribs and at focus using boundary element formulation and constrained optimisation.[25]

6.6.7 Nonlinear models for ultrasound wave propagation in soft tissue

When the peak pressures of the wave is large, energy will be transferred from the fundamental to higher harmonics. As has been described previously, the absorption of ultrasound is frequency-dependent, so that the higher frequency components will be preferentially absorbed by the medium, leading to higher temperatures. As with linear simulations, the contribution to the thermal field from absorption uses the plane wave assumption, but is given by the sum of the N-harmonics computed

$$q_a = 2\sum_{i}^{N} \frac{\alpha_i p_i^2}{c\rho}. \tag{6.7}$$

A difficulty for the computation of nonlinear wave propagation is how to determine the number of harmonics to compute *a priori* in three-dimensional simulations for efficient memory allocation (or equivalently, the spatial resolution required). One approach is, if possible, to average the initial source condition around the axial direction, so that it is rotationally symmetric and use the KZK equation, which is far more computationally tractable, to provide an estimate for the number of harmonics required in three-dimensional simulations. However, this approach assumes layered media, so may not be applicable in highly complex media.

Neglecting dissipative terms, and considering an integral form of the energy conservation equation around the shock front yields[52]

$$q_s = \frac{\beta}{6\rho^2 c^2} (\Delta P)^3, \tag{6.8}$$

where the shock-height of the pressure wave is denoted by ΔP. Note that the contribution to heating from shock-enhanced heating is *independent* of the attenuation of the medium. For a discussion of this see Pearce[52].

Shock-enhanced heating can play a significant role in thermal therapies, such as boiling histotripsy[62], as it proportional to the cube of the pressure, rather than the square[62,103]. Note that as tissue is a heavily attenuating medium, the shocks have a finite rise-time, rather than an infinite rise-time and discontinuity in pressure. This scenario is less computationally demanding, as the shock can be defined over a few grid points, relaxing restrictions on the spatial resolution.

A key difference between shock-enhanced heating and heating due to nonlinearity is that the shock-enhanced heating is a highly localised effect, whereas the absorption of nonlinear ultrasound, although may only be significant in the vicinity of the focus, is, strictly speaking, global effect. That is one must determine whether a shock-like wave has formed or not in order to compute any thermal contributions from shock-enhanced heating. The defining feature is that above a threshold initial pressure, the rise-time is independent of the driving voltage.

There are two approaches to computing shock-like waves in therapeutic ultrasound: the first is to employ operator-splitting[104] and handle the nonlinearity operator using a high-resolution shock capturing scheme[71,105], the second is to compute both the pressure and velocity fields, and formulate the governing equations as a hyperbolic equation by retaining the second-order Lagrangian density[106]

$$\frac{\partial \rho}{\partial t} + \nabla \cdot (\rho \mathbf{u}) = 0 \tag{6.9a}$$

$$\frac{\partial (\rho \mathbf{u})}{\partial t} + \nabla \cdot \left(\rho_0 \mathbf{u} \times \mathbf{u} + I \left(c_0^2 \rho + \frac{c_0^2}{\rho_0} (\beta - 1) (\rho - \rho_0)^2 \right) \right) = \rho_0 \nabla^2 \mathbf{u} \tag{6.9b}$$

An advantage of the first approach is that the number of variables required does not change from standard models, nor are any additional material properties required. Another advantage is that by retaining the structure of the Westervelt equation, computationally efficient forward propagation methods can be used for attenuation and diffraction. However, a disadvantage is that the use of operator-splitting techniques may reduce the overall spatial accuracy of the scheme unless techniques such as Strang-splitting[104,107] are employed.

Shock capturing methods usually exploit the hyperbolic structure of the governing equation. The benefit of this is that many modern high-resolution shock-capturing schemes exploit the conservation laws inherent in the hyperbolic formulation. Such approaches use upwind-type differencing schemes, which perform differencing based on local wave speeds, to discretise the equations with the high spatial resolution required for steep gradients associated with shock-like waves. Another advantage is that the computation of the absorption term no longer relies on the quasi-plane wave assumption which may break down at interfaces in which there is a significant change in impedance. Also, through the inclusion of the second-order Lagrangian density term, the governing equation can be considered in a sense more general than the Westervelt equation, with the ability to model the interaction between waves of differing frequency. However, although there some uses of parametric arrays in therapeutic ultrasound[108], it is not widespread.

One caveat is that many of therapeutic applications which exploit shock-enhanced heating do so in order to harness the mechanical damage caused by clouds of inertially collapsing bubbles. At present, there are no established measures of dose to describe fractionation cause by bubble clouds. Care is needed in modelling the interaction between the bubble cloud and the acoustic field, as the shockwave scatterer and reflection can lead to prefocal constructive interference which can initiate nucleation[66]

6.7 Summary

This chapter discusses the range of factors which influence the selection of numerical scheme for acoustic wave simulations. The table summarises the factors which influences the selection of a numerical scheme for acoustic simulation.

There are three key factors to consider for modelling:

TABLE 6.1
Summary of the factors which influence choice of numerical schemes

	Duration	Motion Management	Intensity	Domain
Histotripsy	Short: time-domain simulation	Exposure durations may be sufficiently short to assume during exposure target is essentially stationary.	High: nonlinear, shock-capturing methods required.	Acoustic wave
Thermal Ablation	Long: continuous-wave simulations	This is target specific, but a judgement on whether motion management is employed must be made.	Moderate: computation of higher harmonics required	Acoustic wave
Transcranial	Moderate: however geometry and techniques to suppress standing waves may restrict assumption of frequency-domain methods which assume continuous wave exposures	No, target may not move a significant amount.	Moderate: however, significant proportion of energy is lost through transmission through the skull. Also transducer design distributes energy over a large area.	Acoustic-elastic wave
Bone Metastases	Long: continuous-wave simulations	Many targets may be considered stationary, however, transcostal applications would require a motion management strategy.	Moderate: computation of higher harmonics required	Acoustic-elastic wave
Hyperthermia	Long: continuous wave simulations	Yes, likely targets will move either due to respiration or drift	Low, linear acoustic simulations may be sufficient	Acoustic wave

- The degree of spatial and temporal inhomogeneity in the medium and the source. This determines whether approximations, such as the paraxial approximation, can be made to reduce the computational complexity of the simulations.
- The intensity of the source. This determines whether nonlinear propagation needs to be modelled, or whether linear models suffice.
- The duration of the exposure time: which determines whether continuous wave exposures, modelled in the frequency-domain, or finite-duration exposures, modelled in the time-domain. A confounding factor is that these features can not be considered in isolation. Consider, for example, the case in which short-pulsed, high-intensities are applied through soft tissue. The first feature means that simulations must be performed in the time domain, the second means that nonlinearity must be considered. Thus, these two features combined require that power-law frequency-dependent attenuation must be handled in the time domain. As mentioned, this can be applied through a fractional Laplacian operator[60] or using a distribution of relaxation processes[57].

Another case is that in which the target may move over the duration of a long hyperthermia treatment. The second factor suggests linear continuous wave methods can be employed, however, the first factor means that solutions should potentially be computed in the time domain. Thus, some analysis must

be preformed to assess the times at which the continuous -wave acoustic field is recomputed to model the change in the position of the target and how this changes the propagation path and consequently the acoustic field. This is both patient and exposure specific.

Table 6.1 outlines which clinical procedures have which features and the potential numerical approaches.

The advantage of frequency-domain simulation methods are that power-law absorption can easily be modelled, although pseudo-spectral time-stepping schemes can handle power-law absorption. Note that if intensity levels are low, nonlinear propagation may be neglected, so frequency-dependence of absorption can also be neglected. However, a limitation of many pseudo-spectral schemes (specifically those which use Fourier basis functions) is that a combination of irregular interfaces and discontinuities in density, such as between soft and hard tissues, poses a numerical challenge.

REFERENCES

1. A. E. Lujan, E. W. Larsen, J. M. Balter, and R. K. Ten Haken. "A method for incorporating organ motion due to breathing into 3D dose calculations". *Med. Phys.* 26.5 (1999), pp. 715–720.
2. P. Wust et al. "Evaluation of segmentation algorithms for generation of patient models in radiofrequency hyperthermia". *Phys. Med. Biol.* 43 (1998), pp. 3295–3307.
3. L. van Wijngaarden. "One-dimensional flow of liquids containing small gas bubbles". *Annu. Rev. Fluid Mech.* 4.1 (1972), pp. 369–396.
4. W. Wiedemair, Ž. Tuković, H. Jasak, D. Poulikakos, and V. Kurtcuoglu. "On ultrasound-induced microbubble oscillation in a capillary blood vessel and its implications for the blood–brain barrier". *Phys. Med. Biol.* 57.4 (2012), pp. 1019–1045.
5. I. M. Hallaj, R. O. Cleveland, and K. Hynynen. "Simulations of the thermo-acoustic lens effect during focused ultrasound surgery". *J. Acoust. Soc. Am.* 109 (2001), pp. 2245–2253.
6. L. Curiel, F. Chavrier, B. Gignoux, S. Pichardo, S. Chesnais, and J.-Y. Chapelon. "Experimental evaluation of lesion prediction modelling in the presence of cavitation bubbles: Intended for high-intensity focused ultrasound prostate treatment". *Med. Bio. Eng. Comp.* 42.1 (2004), pp. 44–54.
7. C. H. Farny, R. G. Holt, and R. A. Roy. "The correlation between bubble-enhanced HIFU heating and cavitation power". *IEEE Trans. Biomed. Eng.* 57.1 (2010), pp. 175–184.
8. S. A. Sapareto and W. C. Dewey. "Thermal dose determination in cancer therapy". *Int. J. Radiat. Oncol. Biol. Phys* 10.6 (1984), pp. 787–800.
9. J. Rogowska. "Overview and fundamentals of medical image segmentation". In: *Handbook of Medical Imaging*. Academic Press, Inc. 2000, pp. 69–85.
10. S. L. Giles. "MR-guided HIFU for pain palliation of bone metastases". *Rad Mag.* 41 (2015), pp. 15–16.
11. Y.-F. Zhou. "High intensity focused ultrasound in clinical tumor ablation". *World J. Clin. Oncol.* 2.1 (2011), pp. 8–27.
12. C. M. C. Tempany, N. J. McDannold, K. Hynynen, and F. A. Jolesz. "Focused ultrasound surgery in oncology: Overview and principles". *Radiology* 259.1 (2011), pp. 39–56.
13. G. Malietzis, L. Monzon, J. Hand, H. Wasan, E. Leen, M. Abel, A. Muhammad, P. Price, and P. Abel. "High-intensity focused ultrasound: Advances in technology and experimental trials support enhanced utility of focused ultrasound surgery in oncology". *Br. J. Radiol.* 86.1024 (2013), p. 20130044.

14. J.-F. Aubry. "High-intensity therapeutic ultrasound: Metrological requirements versus clinical usage". *Metrologia* 49.5 (2012), S259.
15. K. Hynynen and R. M. Jones. "Image-guided ultrasound phased arrays are a disruptive technology for non-invasive therapy". *Phys. Med. Biol.* 61.17 (2016), R206.
16. A. Pulkkinen, B. Werner, E. Martin, and K. Hynynen. "Numerical simulations of clinical focused ultrasound functional neurosurgery". *Phys. Med. Biol.* 59.7 (2014), pp. 1679–1700.
17. A. Scherrer, S. Jakobsson, and K.-H. Küfer. "On the advancement and software support of decision-making in focused ultrasound therapy". *J. Multi.-Crit. Decis. Anal.* 23.5-6 (2016), pp. 174–182.
18. A. Scherrer, S. Jakobsson, A. Belyaev, A. Hoffmann, M. Bortz, X. R. Reit, and K.-H. Küfer. "A hybrid optimization method for focused ultrasound plan computation". *Berichte des Fraunhofer ITWM (Reports of Fraunhofer ITWM)* 249 (2016).
19. C. Uhler and S. J. Wright. "Packing ellipsoids with overlap". *SIAM Rev.* 55.4 (2013), pp. 671–706.
20. R. J. Fedewa, R. Seip, R. F. Carlson, W. Chen, N. T. Sanghvi, M. A. Penna, K. A. Dines, and R. E. Pfile. "Automated treatment planning for prostate cancer HIFU therapy". In: *2005 IEEE Int. Ultrasonics Symp. Proc.* 2005, pp. 1135–1138.
21. J. Coon, A. Payne, and R. Roemer. "HIFU treatment time reduction in superficial tumours through focal zone path selection". *Int. J. Hyperthermia* 27.5 (2011), pp. 465–481.
22. M. Malinen, T. Huttunen, J. P. Kaipio, and K. Hynynen. "Scanning path optimization for ultrasound surgery". *Phys. Med. Biol.* 50.15 (2005), pp. 3473–3490.
23. T. D. Khokhlova and J. H. Hwang. "HIFU for palliative treatment of pancreatic cancer". *J. Gastrointest. Oncol.* 2.3 (2011), pp. 175–184.
24. R. Ritchie, J. Collin, C. Coussios, and T. Leslie. "Attenuation and de-focusing during high-intensity focused ultrasound therapy through peri-nephric fat". *Ultrasound Med. Biol.* 39.10 (2013), pp. 1785–1793.
25. P. Gélat, G. ter Haar, and N. Saffari. "Modelling of the acoustic field of a multi-element HIFU array scattered by human ribs". *Phys. Med. Biol.* 56 (2011), pp. 5553–5581.
26. F. Marquet, J.-F. Aubry, M. Pernot, M. Fink, and M. Tanter. "Optimal transcostal high-intensity focused ultrasound with combined real-time 3D movement tracking and correction". *Phys. Med. Biol.* 56 (2011), pp. 7061–7080.
27. Z. Wu, E. Rietzel, V. Boldea, D. Sarrut, and G. C. Sharp. "Evaluation of deformable registration of patient lung 4DCT with subanatomical region segmentations". *Med. Phys.* 35.2 (2008), pp. 775–781.
28. K. K. Brock, M. B. Sharpe, L. A. Dawson, S. M. Kim, and D. A. Jaffray. "Accuracy of finite element model-based multi-organ deformable image registration". *Med. Phys.* 32.6 (2005), pp. 1647–1659.
29. A. Al-Mayah, J. Moseley, M. Velec, and K. K. Brock. "Sliding characteristic and material compressibility of human lung: Parametric study and verification". *Med. Phys.* 36.10 (2009), pp. 4625–4633.
30. A. Schmidt-Richberg, R. Werner, H. Handels, and J. Ehrhardt. "Estimation of slipping organ motion by registration with direction-dependent regularization". *Med. Image Anal.* 16.1 (2012), pp. 150–159.
31. M. Schwenke, J. Georgii, and T. Preusser. "Fast numerical simulation of focused ultrasound treatments during respiratory motion with discontinuous motion boundaries". *IEEE Trans. Biomed. Eng.* 64.7 (2017), pp. 1455–1468.

32. O. Lorton et al. "Self-scanned HIFU ablation of moving tissue using real-time hybrid US-MR imaging". *IEEE Trans. Biomed. Eng.* 66.8 (2018), pp. 2182–2191.
33. D. Fontanarosa, S. Van der Meer, J. Bamber, E. Harris, T. O'Shea, and F. Verhaegen. "Review of ultrasound image guidance in external beam radiotherapy: I. Treatment planning and inter-fraction motion management". *Phys. Med. Biol.* 60.3 (2015), R77.
34. F. Wu, Z.-B. Wang, Y.-D. Cao, Q. Zhou, Y. Zhang, Z.-L. Xu, and X.-Q. Zhu. "Expression of tumor antigens and heat-shock protein 70 in breast cancer cells after high-intensity focused ultrasound ablation". *Ann. Surg. Oncol.* 14.3 (2007), pp. 1237–1242.
35. F. A. Duck. *Physical Properties of Tissue: A Comprehensive Reference Book*. London: Academic Press, 1990.
36. M. A. Lewis, R. M. Staruch, and R. Chopra. "Thermometry and ablation monitoring with ultrasound". *Int. J. Hyperthermia* 31.2 (2015), pp. 163–181.
37. E. Neufeld, A. Kyriacou, W. Kainz, and N. Kuster. "Approach to validate simulation-based distribution predictions combining the Gamma-method and uncertainty assessment: Application to focused ultrasound". *J. Verif. Valid. Uncert.* 1.3 (2016), p. 031006.
38. T. E. Vaughan and K. Hynynen. "Effects of parameter errors in the simulation of transcranial focused ultrasound". *Phys. Med. Biol.* 47.1 (2001), pp. 37–45.
39. V. Suomi, J. Jaros, B. Treeby, and R. Cleveland. "Nonlinear 3-D simulation of high-intensity focused ultrasound therapy in the kidney". In: *38th Annual International Conference of the IEEE Engineering in Medicine and Biology Society (EMBC)*. IEEE. 2016, pp. 5648–5651.
40. C. W. Connor and K. Hynynen. "Bio-acoustic thermal lensing and nonlinear propagation in focused ultrasound surgery using large focal spots: A parametric study". *Phys. Med. Biol.* 47 (2002), pp. 1911–1928.
41. G. T. Clement and K. Hynynen. "A non-invasive method for focusing ultrasound through the human skull". *Phys. Med. Biol.* 47.8 (2002), pp. 1219–1236.
42. A. Payne et al. "AAPM Task Group 241: A medical physicist's guide to MRI-guided focused ultrasound body systems". *Med. Phys.* 48.9 (2021), e772–e806.
43. T. N. Erpelding, K. W. Hollman, and M. O'Donnell. "Bubble-based acoustic radiation force using chirp insonation to reduce standing wave effects". *Ultrasound Med. Biol.* 33.2 (2007), pp. 263–269.
44. S. C. Tang and G. T. Clement. "Acoustic standing wave suppression using randomized phase-shift-keying excitations". *J. Acoust. Soc. Am.* 126.4 (2009), pp. 1667–1670.
45. W. M. Whelan, D. R. Wyman, and B. C. Wilson. "Investigations of large vessel cooling during interstitial laser heating". *Med. Phys.* 22 (1995), pp. 105–115.
46. C. D. Mann, M. S. Metcalfe, D. M. Lloyd, G. J. Maddern, and A. R. Dennison. "The safety and efficacy of ablative techniques adjacent to the hepatic vasculature and biliary system". *ANZ J. Surg.* 80.1-2 (2010), pp. 41–49.
47. K. Hynynen, A. H. Chung, V. Colucci, and F. A. Jolesz. "Potential adverse effects of high-intensity focused ultrasound exposure on blood vessels *in vivo*". *Ultrasound Med. Biol.* 22.2 (1996), pp. 193–201.
48. T. Kamakura, K. Matsuda, Y. Kumamoto, and M. A. Breazeale. "Acoustic streaming induced in focused Gaussian beams". *J. Acoust. Soc. Am.* 97.5 (1995), pp. 2740–2446.

49. M. A. Solovchuk, T. W. H. Sheu, W. L. Lin, I. Kuo, and M. Thiriet. "Simulation study on acoustic streaming and convective cooling in blood vessels during a high-intensity focused ultrasound thermal ablation". *Int. J. Heat Mass Transfer* 55 (4 2011), pp. 1261–1270.
50. M. F. Hamilton and D. T. Blackstock. *Nonlinear Acoustics*. San Diego, CA: Academic Press, 1998.
51. H. H. Pennes. "Analysis of tissue and arterial blood temperatures in the resting human forearm". *J. Appl. Physiol.* 1.2 (1948), pp. 93–122.
52. A. D. Pierce. *Acoustics: An Introduction to Its Physical Principles and Applications*. New York: American Institute of Physics, 1989.
53. I. Christov, C. I. Christov, and P. M. Jordan. "Modeling weakly nonlinear acoustic wave propagation". *Quart. J. Mech. Appl. Math.* 60.4 (2007), pp. 473–496.
54. V. P. Kuznetsov. "Equations of nonlinear acoustics". *Sov. Phys. Acoust.* 16 (1971), pp. 467–470.
55. S. I. Aanonsen, T. Barkve, J. Naze-Tjøtta, and S. Tjøtta. "Distortion and harmonic generation in the nearfield of a finite amplitude sound beam". *J. Acoust. Soc. Am.* 75 (1984), pp. 749–768.
56. P. J. Westervelt. "Parametric acoustic array". *J. Acoust. Soc. Am.* 35 (1963), pp. 535–537.
57. G. Pinton, J. Dahl, S. Rosenzweig, and G. Trahey. "A heterogeneous nonlinear attenuating full-wave model of ultrasound". *IEEE Trans. Ultrason., Ferroelect., Freq. Contr.* 56.3 (2009), pp. 474–488.
58. A. A. Doinikov, A. Novell, P. Calmon, and A. Bouakaz. "Simulations and measurements of 3-D ultrasonic fields radiated by phased-array transducers using the Westervelt equation". *IEEE Trans. Ultrason., Ferroelect., Freq. Contr.* 61.9 (2014), pp. 1470–1477.
59. W. Chen and S. Holm. "Fractional Laplacian time-space models for linear and nonlinear lossy media exhibiting arbitrary frequency power-law dependency". *J. Acoust. Soc. Am.* 115.4 (2004), pp. 1424–1430.
60. B. E. Treeby and B. T. Cox. "Modeling power law absorption and dispersion for acoustic propagation using the fractional Laplacian". *J. Acoust. Soc. Am.* 127 (2010), pp. 2741–2748.
61. T. L. Szabo. "Time domain wave equations for lossy media obeying a frequency power law". *J. Acoust. Soc. Am.* 96.1 (1994), pp. 491–500.
62. M. S. Canney, M. R. Bailey, L. A. Crum, V. A. Khokhlova, and O. A. Sapozhnikov. "Acoustic characterization of high intensity focused ultrasound fields: A combined measurement and modeling approach". *J. Acoust. Soc. Am.* 124.4 (2008), pp. 2406–2420.
63. J. E. Soneson. "A parametric study of error in the parabolic approximation of focused axisymmetric ultrasound beams". *J. Acoust. Soc. Am.* 131.6 (2012), EL481–EL486.
64. E. G. Lobanova, S. V. Lobanov, and V. A. Khokhlova. "Counterpropagation of waves with shock fronts in a nonlinear tissue-like medium". *Acoust. Phys.* 60.4 (2014), pp. 387–397.
65. A. S. Sangani. "A pairwise interaction theory for determining the linear acoustic properties of dilute bubbly liquids". *J. Fluid Mech.* 232 (1991), pp. 221–284.
66. K. J. Pahk, S. Lee, P. Gélat, M. Oliveira de Andrade, and N. Saffari. "The interaction of shockwaves with a vapour bubble in boiling histotripsy: The shock scattering effect". *Ultrason. Sonochem.* 70 (2021), p. 105312.
67. P. J. White, G. T. Clement, and K. Hynynen. "Longitudinal and shear mode ultrasound propagation in human skull bone". *Ultrasound Med. Biol.* 32.7 (2006), pp. 1085–1096.

68. M. D. J. McGarry, C. L. Johnson, B. P. Sutton, J. G. Georgiadis, E. E. W. Van Houten, A. J. Pattison, J. B. Weaver, and K. D. Paulsen. "Suitability of poroelastic and viscoelastic mechanical models for high and low frequency MR elastography". *Med. Phys.* 42.2 (2015), pp. 947–957.
69. P. R. Perriñez, F. E. Kennedy, E. E. W. Van Houten, J. B. Weaver, and K. D. Paulsen. "Modeling of soft poroelastic tissue in time-harmonic MR elastography". *IEEE Trans. Biomed. Eng.* 56.3 (2009), pp. 598–608.
70. O. A. Sapozhnikov, S. A. Tsysar, V. A. Khokhlova, and W. Kreider. "Acoustic holography as a metrological tool for characterizing medical ultrasound sources and fields". *J. Acoust. Soc. Am.* 138.3 (2015), pp. 1515–1532.
71. P. V. Yuldashev and V. A. Khokhlova. "Simulation of three-dimensional nonlinear fields of ultrasound therapeutic arrays". *Acoust. Phys.* 57.3 (2011), pp. 334–343.
72. J. Gu and Y. Jing. "A modified mixed domain method for modeling acoustic wave propagation in strongly heterogeneous media". *J. Acoust. Soc. Am.* 147.6 (2020), pp. 4055–4068.
73. O. P. Bruno, Y. Han, and M. M. Pohlman. "Accurate, high-order representation of complex three-dimensional surfaces via Fourier continuation analysis". *J. Comput. Phys.* 227.2 (2007), pp. 1094–1125.
74. Y. Jing and G. T. Clement. "On the use of Gegenbauer reconstructions for shock wave propagation modeling". *J. Acoust. Soc. Am.* 130 (2011), pp. 1115–1124.
75. J. P. Berenger. "A perfectly matched layer for the absorption of electromagnetic waves". *J. Comput. Phys.* 114 (1994), pp. 185–200.
76. Q.-H. Liu and J. Tao. "The perfectly matched layer for acoustic waves in absorptive media". *J. Acoust. Soc. Am.* 102 (1997), pp. 2072–2082.
77. G. Mur. "Absorbing boundary conditions for the finite-difference approximation of the time-domain electromagnetic-field equations". *IEEE Trans. Electromagn. Compat.* 4 (1981), pp. 377–382.
78. M. M. Chen and K. R. Holmes. "Microvascular contributions in tissue heat transfer". *Ann. NY Acad. Sci.* 335.1 (1980), pp. 137–150.
79. K. H. Keller and L. Seiler. "An analysis of peripheral heat transfer in man". *J. Appl. Physiol.* 30 (1971), pp. 779–786.
80. P. Deuflhard and R. Hochmuth. "Multiscale analysis of thermoregulation in the human microvascular system". *Math. Meth. Appld Sci.* 27.8 (2004), pp. 971–989.
81. G. M. J. V. Leeuwen, A. Kotte, B. W. Raaymakers, and J. J. W. Lagendijk. "Temperature simulations in tissue with a realistic computer generated vessel network". *Phy. Med. Biol.* 45 (2000), pp. 1035–1049.
82. S. Weinbaum and L. M. Jiji. "A new simplified equation for the effect of blood flow on local average tissue temperature". *ASME J. Biomech. Eng.* 107 (1985), pp. 131–139.
83. K. R. Diller and J. A. Pearce. "Issues in modeling thermal alterations in tissues". *Ann. NY Acad. Sci.* 888.1 (1999), pp. 153–164.
84. P. Leuenberger, S. Ganscha, A. Kahraman, V. Cappelletti, P. J. Boersema, C. von Mering, M. Claassen, and P. Picotti. "Cell-wide analysis of protein thermal unfolding reveals determinants of thermostability". *Science* 355.6327 (2017), eaai7825.

85. D. P. O'Neill, T. Peng, P. Stiegler, U. Mayrhauser, S. Koestenbauer, K. Tscheliessnigg, and S. J. Payne. "A three-state mathematical model of hyperthermic cell death". *Ann. Biomed. Eng.* 39.1 (2011), pp. 570–579.

86. Y. Xu and R. Qian. "Analysis of thermal injury process based on enzyme deactivation mechanisms". *J. Biomech. Eng.* 117.4 (1995), pp. 462–465.

87. S. Singh and R. Melnik. "Coupled thermo-electro-mechanical models for thermal ablation of biological tissues and heat relaxation time effects". *Phys. Med. Biol.* 64.24 (2019), p. 245008.

88. J. A. Pearce. "Relationship between Arrhenius models of thermal damage and the CEM 43 thermal dose". In: *Energy-based Treatment of Tissue and Assessment V*. Vol. 7181. International Society for Optics and Photonics. 2009, p. 718104.

89. E. L. Jones, J. R. Oleson, L. R. Prosnitz, T. V. Samulski, Z. Vujaskovic, D. Yu, L. L. Sanders, and M. W. Dewhirst. "Randomized trial of hyperthermia and radiation for superficial tumors". *J. Clin. Oncol.* 23.13 (2005), pp. 3079–3085.

90. A. D. Maxwell, T.-Y. Wang, C. A. Cain, J. B. Fowlkes, O. A. Sapozhnikov, M. R. Bailey, and Z. Xu. "Cavitation clouds created by shock scattering from bubbles during histotripsy". *J. Acoust. Soc. Am.* 130.4 (2011), pp. 1888–1898.

91. X. Fan and K. Hynynen. "The effect of wave reflection and refraction at soft tissue interfaces during ultrasound hyperthermia treatments". *J. Acoust. Soc. Am.* 91 (1992), pp. 1727–1736.

92. A. Alaniz, F. Kallel, E. Hungerford, and J. Ophir. "Variational method for estimating the effects of continuously varying lenses in HIFU, sonography, and sonography-based cross-correlation methods". *J. Acoust. Soc. Am.* 111 (2002), pp. 468–474.

93. R. J. McGough. "Rapid calculations of time-harmonic nearfield pressures produced by rectangular pistons". *J. Acoust. Soc. Am.* 115.5 (2004), pp. 1934–1941.

94. X. Zeng and R. J. McGough. "Optimal simulations of ultrasonic fields produced by large thermal therapy arrays using the angular spectrum approach". *J. Acoust. Soc. Am.* 125 (2009), pp. 2967–2977.

95. R. J. Zemp, J. Tavakkoli, and R. S. C. Cobbold. "Modeling of nonlinear ultrasound propagation in tissue from array transducers". *J. Acoust. Soc. Am.* 113 (2003), pp. 139–152.

96. U. Vyas and D. Christensen. "Ultrasound beam simulations in inhomogeneous tissue geometries using the hybrid angular spectrum method". *IEEE Trans. Ultrason., Ferroelect., Freq. Contr.* 59.6 (2012), pp. 1093–1100.

97. J. Georgii, C. von Dresky, S. Meier, D. Demedts, C. Schumann, and T. Preusser. "Focused ultrasound - efficient GPU simulation methods for therapy planning". In: *Workshop in Virtual Reality Interactions and Physical Simulation "VRIPHYS" (2011)*. Ed. by J. Bender, K. Erleben, and E. Galin. The Eurographics Association, 2011.

98. J.-J. Gu and Y. Jing. "Modeling of wave propagation for medical ultrasound: A review". *IEEE Trans. Ultrason., Ferroelect., Freq. Contr.* 62.11 (2015), pp. 1979–1992.

99. J. E. Soneson and M. R. Myers. "Thresholds for nonlinear effects in high-intensity focused ultrasound propagation and tissue heating". *IEEE Trans. Ultrason., Ferroelect., Freq. Contr.* 57.11 (2010), pp. 2450–2459.

100. S. P. Groth, P. Gélat, S. R. Haqshenas, N. Saffari, E. van't Wout, T. Betcke, and G. N. Wells. "Accelerating frequency-domain numerical methods for weakly nonlinear focused ultrasound using nested meshes". *J. Acoust. Soc. Am.* 150.1 (2021), pp. 441–453.

101. M. Raissi, P. Perdikaris, and G. E. Karniadakis. "Physics-informed neural networks: A deep learning framework for solving forward and inverse problems involving nonlinear partial differential equations". *J. Comput. Phys.* 378 (2019), pp. 686–707.

102. A. Stanziola, S. R. Arridge, B. T. Cox, and B. E. Treeby. "A Helmholtz equation solver using unsupervised learning: Application to transcranial ultrasound". *J. Comput. Phys.* 441 (2021), p. 110430.

103. O. V. Bessonova, V. A. Khokhlova, M. S. Canney, M. R. Bailey, and L. A. Crum. "Focusing of high power ultrasound beams and limiting values of shock wave parameters". *Acoust. Phys.* 55.4 (2009), pp. 463–473.

104. W. Hundsdorfer and J. G. Verwer. *Numerical Solution of Time-Dependent Advection-Diffusion-Reaction Equations*. Vol. 33. Springer, 2003.

105. A. Kurganov and E. Tadmor. "New high-resolution central schemes for nonlinear conservation laws and convection–diffusion equations". *J. Comput. Phys.* 160.1 (2000), pp. 241–282.

106. R. Velasco-Segura and P. L. Rendón. "A finite volume approach for the simulation of nonlinear dissipative acoustic wave propagation". *Wave Motion* 58 (2015), pp. 180–195.

107. G. Strang. "On the construction and comparison of difference schemes". *SIAM J. Numer. Anal.* 5.3 (1968), pp. 506–517.

108. E. Konofagou, J. Thierman, and K. Hynynen. "A focused ultrasound method for simultaneous diagnostic and therapeutic applications - A simulation study". *Phys. Med. Biol.* 46.11 (2001), pp. 2967–2984.